Highly sensitive dispersion measurement of a high-power passive optical resonator using spatial-spectral interferometry

Ioachim Pupeza[1,*], Xun Gu[1], Ernst Fill[1], Tino Eidam[2], Jens Limpert[2], Andreas Tünnermann[2], Ferenc Krausz[1], and Thomas Udem[1]

[1] *Max-Planck-Institut für Quantenoptik, Hans-Kopfermann-Str. 1, 85748 Garching, Germany*
[2] *Friedrich-Schiller-Universität Jena, Institut für Angewandte Physik, Albert-Einstein-Str. 15, 07745 Jena, Germany*

**ioachim.pupeza@mpq.mpg.de*

Abstract: We apply spatially and spectrally resolved interferometry to measure the complex ratio between the field circulating inside a high-finesse femtosecond enhancement cavity and the seeding field. Our simple and highly sensitive method enables the measurement of single-round-trip group delay dispersion of a fully loaded cavity at resonance for the first time. Group delay dispersion can be determined with a reproducibility better than 1 fs^2 allowing the investigation of nonlinear processes triggered by the high intracavity power. The required data acquisition time is less than 1 s.

OCIS codes: (140.4050) Mode-locked lasers; (120.0120) Instrumentation, measurement, and metrology; (320.7100) Ultrafast measurements; (230.5750) Resonators.

References and links

1. G. Rempe, R. J. Thompson, H. J. Kimble, and R. Lalezari, "Measurement of ultralow losses in an optical interferometer," Opt. Lett. **17,** 363–365 (1992).
2. C. Gohle, Th. Udem, M. Herrmann, J. Rauschenberger, R. Holzwarth, H. A. Schuessler, F. Krausz, and T. W. Hänsch, "A frequency comb in the extreme ultraviolet," Nature **436,** 234–237 (2005).
3. R. J. Jones, K. D. Moll, M. J. Thorpe, and J. Ye, "Phase-Coherent Frequency Combs in the Vacuum Ultraviolet via High-Harmonic Generation inside a Femtosecond Enhancement Cavity," Phys. Rev. Lett. **94,** 193201 (2005).
4. A. Ozawa, J. Rauschenberger, C. Gohle, M. Herrmann, D. R. Walker, V. Pervak, A. Fernandez, R. Graf, A. Apolonski, R. Holzwarth, F. Krausz, T. W. Hänsch, and Th. Udem, "High Harmonic Frequency Combs for High Resolution Spectroscopy," Phys. Rev. Lett. **100,** 253901 (2008).
5. D. C. Yost, T. R. Schibli, and J. Ye, "Efficient output coupling of intracavity high harmonic generation," Opt. Lett. **33,** 1099–1101 (2008).
6. I. Hartl, T. R. Schibli, A. Marcinkevicius, D. C. Yost, D. D. Hudson, M. E. Fermann, and J. Ye, "Cavity-enhanced similariton Yb-fiber laser frequency comb: 3×10^{14} W/cm^2 peak intensity at 136MHz," Opt. Lett. **32,** 2870–2872 (2007).
7. M. Hentschel, Z. Cheng, F. Krausz, and Ch. Spielmann, "Generation of 0.1-TW optical pulses with a single-stage Ti:sapphire amplifier at a 1-kHz repetition rate," Appl. Phys. B **70,** 161–164 (2000).
8. F. X. Kaertner, W. S. Graves, D. E. Moncton, and F. O. Ilday, US Patent Application Publication US2006/0251217 A1 (2006).
9. F. V. Hartemann, W. J. Brown, D. J. Gibson, S. G. Anderson, A. M. Tremaine, P. T. Springer, A. J. Wootton, E. P. Hartouni, and C. P. J. Barty, "High-energy scaling of Compton scattering light sources," Phys. Rev. Spec. Top. Acc. Beams **8,** 100702 (2005).
10. M. Theuer, D. Molter, K. Maki, C. Otani, J. A. Lhuillier, and R. Beigang, "Terahertz generation in an actively controlled femtosecond enhancement cavity," Appl. Phys. Lett. **93,** 041119 (2008).
11. A. N. Luiten and J. C. Petersen, "Ultrafast resonant polarization interferometry: Towards the first direct detection of vacuum polarization," Phys. Rev. A **70,** 033801 (2004).

#132118 - $15.00 USD Received 22 Jul 2010; revised 30 Sep 2010; accepted 16 Oct 2010; published 1 Dec 2010

12. R. G. DeVoe, C. Fabre, K. Jungmann, J. Hoffnagle, and R. G. Brewer, "Precision Optical-Frequency- Difference Measurements," Phys. Rev. A **37**, 1802–1805 (1988).
13. C. J. Hood, H. J. Kimble, and J. Ye, "Characterization of high-finesse mirrors: Loss, phase shifts, and mode structure in an optical cavity," Phys. Rev. A **64**, 033804 (2001).
14. B. Bernhardt, A. Ozawa, P. Jacquet, M. Jacquey, Y. Kobayashi, T. Udem, R. Holzwarth, G. Guelachvili, T. W. Hänsch, and N. Picqué, "Cavity-enhanced dual-comb spectroscopy," Nat. Photonics **4,** 55–57 (2010).
15. M. Thorpe, R. Jones, K. Moll, J. Ye, and R. Lalezari, "Precise measurements of optical cavity dispersion and mirror coating properties via femtosecond combs," Opt. Express **13,** 882–888 (2005).
16. A. Schliesser, C. Gohle, T. Udem, and T. W. Hänsch, "Complete characterization of a broadband high-finesse cavity using an optical frequency comb," Opt. Express **14,** 5975–5983 (2006).
17. C. Gohle, B. Stein, A. Schliesser, T. Udem, and T. W. Hänsch, "Frequency Comb Vernier Spectroscopy for Broadband, High-Resolution, High-Sensitivity Absorption and Dispersion Spectra," Phys. Rev. Lett. **99,** 263902 (2007).
18. T. J. Hammond, A. K. Mills, and D. J. Jones, "Simple method to determine dispersion of high-finesse optical cavities," Opt. Express **17,** 8998–9005 (2009).
19. I. Pupeza, T. Eidam, J. Rauschenberger, B. Bernhardt, A. Ozawa, E. Fill, A. Apolonski, Th. Udem, J. Limpert, Z. A. Alahmed, A. M. Azzeer, A. Tünnermann, T. W. Hänsch, and F. Krausz, "Power scaling of a high repetition rate enhancement cavity," Opt. Lett. **12,** 2052–2054 (2010).
20. A. P. Kovács, K. Osvay, Zs. Bor, and R. Szipöcs, "Group-delay measurement on laser mirrors by spectrally resolved white-light interferometry," Opt. Lett. **20,** 788–790 (1995).
21. D. Meshulach, D. Yelin, and Y. Silberberg, "Real-time spatialspectral interference measurements of ultrashort optical pulses," J. Opt. Soc. Am. B, **14,** 2095–2098 (1997).
22. P. Bowlan, P. Gabolde, M. A. Coughlan, R. Trebino, and R. J. Levis, "Measuring the spatiotemporal electric field of ultrashort pulses with high spatial and spectral resolution," J. Opt. Soc. Am. B **25,** A81–A92 (2008).
23. A. Börzsönyi, A. P. Kovács, M. Görbe, and K. Osvay, "Advances and limitations of phase dispersion measurement by spectrally and spatially resolved interferometry," Opt. Commun. **281,** 3051–3061 (2008).
24. D. E. Adams, T. A. Planchon, A. Hrin, J. A. Squier, and C. G. Durfee, "Characterization of coupled nonlinear spatiospectral phase following an ultrafast self-focusing interaction," Opt. Lett. **34,** 1294–1296 (2009).
25. K. Osvay, A. Börzsönyi, A. P. Kovács, M. Görbe, G. Kurdi, and M. P. Lalashnikov, "Dispersion of femtosecond laser pulses in beam pipelines from ambient pressure to 0.1 mbar," Appl. Phys. B **87,** 457–461 (2007).
26. A. Börzsönyi, Z. Heiner, M. P. Kalashnikov, A. P. Kovács, and K. Osvay, "Dispersion measurement of inert gases and gas mixtures at 800 nm," Appl. Opt. **47,** 4856–4863 (2008).
27. K. Osvay, L. Canova, C. Durfee, A. P. Kovács, Á. Börzsönyi, O. Albert, and R. Lopez Martens, "Preservation of the carrier envelope phase during cross-polarized wave generation," Opt. Express **25,** 22358–22365 (2009).
28. D. E. Adams, T. A. Planchon, J. A. Squier, and C. G. Durfee, "Spatiotemporal dynamics of cross-polarized wave generation," Opt. Lett. **35,** 1115–1117 (2010).
29. K. Osvay, Á. Börzsönyi, Z. Heiner, A. P. Kovács, and M. P. Kalashnikov, "Measurement of Pressure Dependent Nonlinear Refractive Index of Inert Gases," CLEO 2009, paper CMU7.
30. T. Eidam, F. Röser, O. Schmidt, J. Limpert and A. Tünnermann, "57 W, 27 fs pulses from a fiber laser system using nonlinear compression," Appl. Phys. B **92,** 9–12 (2008).
31. T. W. Hänsch and B. Couillaud, "Laser Frequency Stabilization by Polarization Spectroscopy of a Reflecting Reference Cavity," Opt. Commun. **35,** 441 (1980).
32. C. Froehly, A. Lacourt, and J. C. Vienot, "Time impulse response and time frequency response of optical pupils," Nouv. Rev. Opt. **4,** 183-196 (1973).
33. L. Lepetit, G. Cheriaux, and M. Joffre, "Linear techniques of phase measurement by femtosecond spectral interferometry for applications in spectroscopy," J. Opt. Soc. Am. B **12,** 24672474 (1995).
34. Th. Udem, R. Holzwarth, and T. W. Hänsch, "Optical frequency metrology," Nature **16,** 233–237 (2002).
35. E. D. Peck and K. Reeder, "Dispersion of Air," J. Opt. Soc. Am. **62,** 958–962 (1972).

1. Introduction

Enhancement cavities are frequently used to increase the efficiency of nonlinear interactions such as second-harmonic generation (SHG). For near-infrared continuous wave lasers, cavities with a finesse approaching 10^6 have been demonstrated [1], albeit with a rather low input power. Recently, efforts to resonantly enhance pulsed lasers have been boosted by the prospect of intracavity high-harmonic generation (HHG) with multi-MHz repetition rates [2–6]. While traditional methods of generating peak intensities exceeding 10^{13} W/cm^2 required for HHG rely on a largely reduced pulse repetition rate (see, for example, [7] and references therein), the intracavity HHG approach can preserve the original repetition rate of the pulsed laser source.

#132118 - $15.00 USD Received 22 Jul 2010; revised 30 Sep 2010; accepted 16 Oct 2010; published 1 Dec 2010

Other proposed applications, for which enhancement cavities constitute a very promising approach, are the generation of high-brilliance hard X-rays via inverse Compton scattering [8, 9], THz generation [10] and the detection of the birefringence of vacuum [11].

Enhancing the power of a train of pulses in an optical resonator requires the constructive interference of the intracavity field with the seeding laser field inside the cavity. In the frequency domain this means that the seeding frequency comb and the cavity resonances have to be matched over the optical bandwidth of interest. While the mode spacing of the seeding mode-locked laser can be assumed to be perfectly regular, the cavity free spectral range may be irregular due to dispersion. In a high-finesse cavity, the effect of single-round-trip dispersion is accumulated over many round trips in the resonant state. This typically restricts the power enhancement to a limited spectral range and therefore needs to be precisely measured and compensated for optimum enhancement. Conversely, the same effect enables highly accurate dispersion [12, 13] and absorption measurements [14].

In the past few years, several approaches to measuring the intracavity dispersion of femtosecond enhancement cavities have been presented [15–18]. All these techniques rely on a controlled variation of the seeding frequency comb and the subsequent interpretation of the cavity response. In [15] and [16], a limited number of modes of the seeding comb is locked to the cavity. In the locked state, either the repetition frequency [16] or the carrier-envelope-offset frequency [15] of the seeding comb is varied and the intracavity spectrum is recorded. Suitable linear cavity models are fitted to the acquired 2-dimensional data sets. Due to the accumulation of dispersion over many cavity round trips, the group delay dispersion (GDD) can be detected with very good sensitivity and a reproducibility on the order of 1 fs^2 is achieved. However, the necessary variation of the seeding comb allows only a few modes to resonate at once, such that these methods are limited to the measurement of the linear cavity response. Thus, they are not suitable for the investigation of average- and peak power-related intracavity effects. In [17] and [18] the authors present techniques in which the frequency comb is scanned through the cavity resonances without locking the laser and the cavity. Even if a steady state is not necessarily reached in the cavity, comparable GDD measurement accuracies are reported. However, these methods are also limited to the linear case. For applications of enhancement cavities involving high peak powers, the restriction of dispersion measurement methods to low power levels is rather severe. Peak-power-dependent enhancement behavior has been reported in HHG cavities [4] including a gas target and an XUV output coupler and even in empty cavities [19]. A phase-sensitive measurement method suitable also for regimes beyond linear enhancement is highly desirable and described in this work.

We employ spatially and spectrally resolved interferometry (SSI) [20–29] to measure the phase difference between the intracavity circulating field and the seeding field. Together with the spectrally resolved power enhancement, this measurement provides full information on the cavity response. This method has several major advantages: for phase retrieval over the entire enhanced bandwidth the seeding comb need not be varied. In particular, this enables the investigation of effects related to high intracavity peak power. The experimental setup is simple and the total measurement time is only limited by the cavity build-up time. Once the cavity reaches the steady state, a single-pulse acquisition is sufficient for an accurate cavity response determination. This provides an increased robustness against jitter effects. We present experimental results for both the linear and nonlinear enhancement regimes, demonstrating sensitivities and reproducibilities comparable to those reported in previous works for linear enhancement.

#132118 - $15.00 USD Received 22 Jul 2010; revised 30 Sep 2010; accepted 16 Oct 2010; published 1 Dec 2010

2. Experimental Setup and Phase Measurement Method

2.1. The Steady State and the Desired Information

Consider an enhancement cavity in the steady state. Let ω denote the angular optical frequency. Let $\widetilde{E}_i(\omega)$ and $\widetilde{E}_c(\omega)$ denote the complex frequency-domain input electric field from the seeding laser and the intracavity circulating field, respectively, within the enhanced spectral region. The behavior of the cavity is described by the ratio $\widetilde{H}(\omega)$ of the circulating to the incoming field:

$$\widetilde{H}(\omega) = |\widetilde{H}(\omega)| \exp[j\phi(\omega)] = \frac{\widetilde{E}_c(\omega)}{\widetilde{E}_i(\omega)}, \tag{1}$$

where $\phi(\omega)$ is the phase of $\widetilde{H}(\omega)$.

There are two qualitatively different regimes of enhancement. In the linear case, $\widetilde{H}(\omega)$ is independent of the circulating field $\widetilde{E}_c(\omega)$ and merely a property of the cavity. The second regime of enhancement involves intracavity nonlinear processes. Here, the enhancement behavior and, thus, $\widetilde{H}(\omega)$, depends on the intracavity electric field. Nonlinearities may emerge through the interaction of high peak powers with the cavity optics or some intracavity medium, see e.g. [4, 19]. In both cases, the complex function $\widetilde{H}(\omega)$ fully describes the response of the cavity to the input electric field $\widetilde{E}_i(\omega)$. Therefore, the knowledge of $\widetilde{H}(\omega)$ is highly desirable. However, the single-round-trip propagation properties inside the cavity are often of interest.

The magnitude $|\widetilde{H}(\omega)|$ can be derived from the incident and intracavity power spectra. The latter is accessible through the leakage of one of the highly reflective cavity mirrors (e.g. M3 or M8) knowing its spectral transmission function. To quickly and accurately measure the phase $\phi(\omega)$ of $\widetilde{H}(\omega)$ we apply SSI. The experimental setup is presented in Section 2.2. In Section 2.3 we discuss the derivation of the intracavity single-round-trip propagation properties in the steady state from the measured complex function $\widetilde{H}(\omega)$. Section 2.4 discusses the effect of the correspondence between the single-round-trip intracavity phase and $\phi(\omega)$ on the sensitivity of the interferometric measurement. Section 2.5 addresses the interferometer data processing.

2.2. The Experimental Setup

Figure 1 depicts the experimental setup. With the exception of the beamsplitter, the delay line and the imaging spectrometer, the setup is identical to the one described in [19]. The pulses are generated by a passively mode-locked, diode-pumped Yb:KYW oscillator and are amplified in a two-stage fiber-based chirped pulse amplifier system. The stretcher and compressor are implemented with transmission gratings. At the output, the 78 MHz repetition rate pulse train reaches up to 50 W of average power. The central wavelength is 1042 nm. By varying the distance between the two compressor gratings, the pulse duration can be adjusted between 200 fs, corresponding to almost bandwidth-limited pulses, and more than 10 ps with a negligible effect on other beam parameters. The laser system is described in detail in [30]. Similar to the systems presented in [2–6], our enhancement cavity is a ring resonator whose round-trip time is adjusted to the inverse of the seeding laser repetition rate. The beam is folded several times for compactness and convenient handling. The cavity is placed inside a vacuum chamber to minimize GDD and losses. All eight dielectric cavity mirrors have low dispersion. The reflectivity of mirrors M2-M8 was determined with a ring-down measurement to be 99.995%$\pm$20ppm, per mirror. Mirror M1 is the input coupler (IC) of the cavity and has a measured reflectivity of 99.887%, M5 and M6 have a radius of curvature of 150 mm and enclose a $w_0 = 22$ μm cavity focus ($1/e^2$-intensity radius calculated for the center of the stability range). The laser transverse mode is matched to the cavity mode with a telescope. As described in [19], a stable lock of the seeding

#132118 - $15.00 USD Received 22 Jul 2010; revised 30 Sep 2010; accepted 16 Oct 2010; published 1 Dec 2010

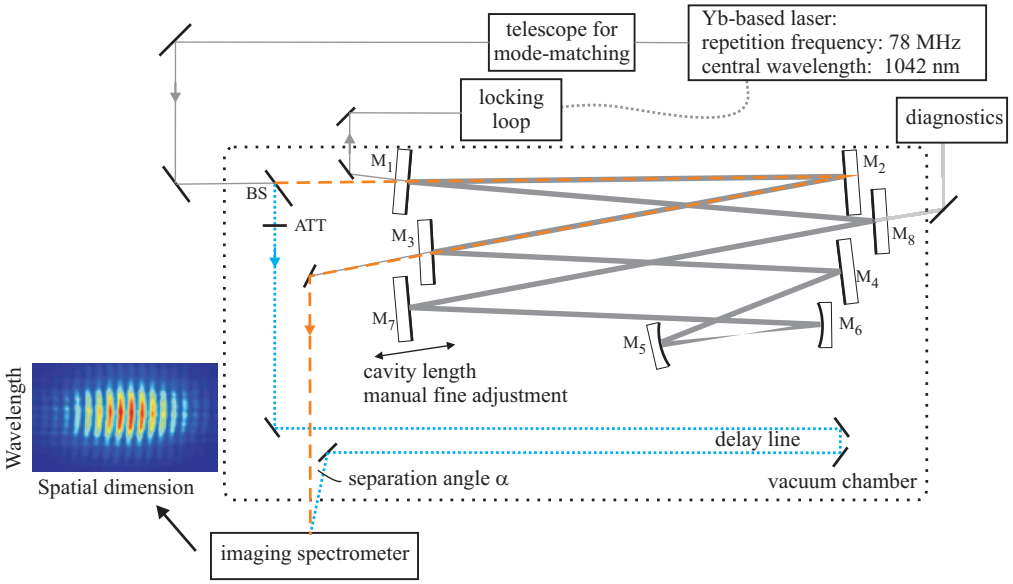

Fig. 1. Experimental setup. BS: beam splitter, blue dotted line: reference beam, orange dashed line: intracavity beam, leaking through the highly reflective mirror M3, ATT: thin neutral density filter attenuation. Diagnostics: photodiode / power meter / spectrometer / autocorrelator.

laser to the enhancement cavity is achieved with the Hänsch-Couillaud scheme [31] controlling the position of an oscillator cavity end mirror mounted on a piezoelectric transducer. For optimum enhancement, an additional coarse adjustment is achieved by manually varying the seed oscillator optical pump power. Typical power enhancement factors range between 1400 and 1800 (see [19]).

To obtain the phase $\phi(\omega)$ of the cavity response function, we use spatially and spectrally resolved interferometry [21–23]. A beamsplitter placed in front of the cavity IC splits off approximately 4% of the input beam (see the blue dotted line in Fig. 1). This beam constitutes the reference arm of the interferometer. The rest of the input beam is sent to and enhanced in the cavity. A copy of the intracavity circulating pulse leaks through the highly reflective mirror M3 (orange dashed line). This beam constitutes the sample arm of the interferometer. Note that throughout the experiments presented in this paper, we assume the constancy of the transmission of mirror M3 with respect to power. The validity of this assumption is confirmed by the observations in [19]. The transmission of M3 amounts to 1.65 ppm. The two arms cross with an angle α at the slit of an imaging spectrometer (model Andor Shamrock 303i using a CCD camera model Andor DV420A-OE). An alternative method for phase retrieval consists in one-dimensional spectral interferometry (SI), see e.g. [32, 33]. For SI, a second beamsplitter could be used to recombine the two interferometer arms collinearly into one beam impinging on a spectrometer, where a 1-dimensional spectral interference fringe pattern is measured. However, SSI offers a better spectral resolution since it avoids the spectral filtering necessary in SI (see e.g. [22]). The time delay $\Delta\tau$ between the two arms can be adjusted with a delay stage implemented in the reference arm. The spatial-spectral interference of the two arms results in a 2-dimensional fringe pattern, which, together with the spectra from the individual interferometer arms, leads to the complete determination of the complex function $\widetilde{H}(\omega)$. The interferometer setup is very flexible in the sense that it allows for arbitrary modifications of the cavity, under

#132118 - $15.00 USD Received 22 Jul 2010; revised 30 Sep 2010; accepted 16 Oct 2010; published 1 Dec 2010

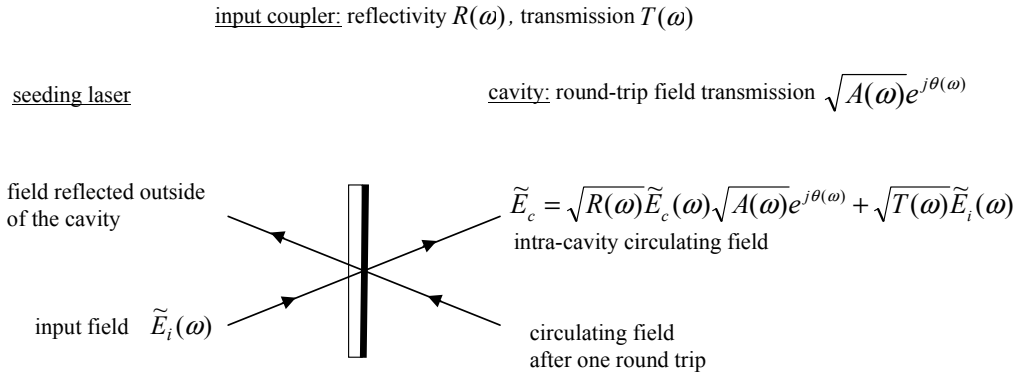

Fig. 2. Electric fields at the input coupler of an enhancement cavity in the steady state.

the constraint that the mirrors M1, M2 and M3 not be displaced. Such modifications may include length and incidence angle variations as well as the exchange of individual mirrors. In particular, the intracavity group delay can be varied by manually displacing mirror M7, i.e. by slightly varying the geometrical cavity length.

To determine $\Delta\tau$, a calibration can be performed while the cavity is off-resonance. For this measurement, we block the cavity beam path without disturbing the propagation in the interferometer sample arm, for instance between mirrors M4 and M5. The delay $\Delta\tau$ is adjusted to 0 by observing the interference fringe spacing. During the measurement, in order to optimize the fringe contrast, the powers in the two interferometer arms are balanced using thin neutral density filters. The GDD imbalance between the two arms can in principle be either corrected using appropriate compensator substrates or numerically removed from the measured phase. In our case, the GDD imbalance owed to a single pass through the substrate of mirror M3 and the neutral density filters amounts to roughly 100 fs^2. However, as will be discussed in Section 2.4, the effect of the cavity round-trip phase on the phase measured in the sample arm of the interferometer is magnified by more than three orders of magnitude due to the resonant enhancement. Therefore, this imbalance introduces a bias of less than 0.1 fs^2 for the determined cavity round-trip GDD and is neglected in the measurements presented here.

A mechanical shutter placed in front of the imaging spectrometer controls the integration time of the measurements. Short integration times are favorable to minimize the effects of amplitude and phase jitter on the recorded data. In the measurements presented here, we used an integration time of approximately 0.5 s, which can be further reduced if needed.

A potential source of systematic uncertainty can be the spatial mode mismatch between the cavity and the reference beams, if the input beam phase front is not perfectly matched to that of the excited transverse cavity mode. In the proof-of-principle experiments presented in this paper, we found it quite reasonable to accept some minor ripples in the retrieved phase, caused by this effect (see Section 3.1). To alleviate this issue and to further increase the accuracy of the measurement, a single-mode input beam is preferred, and additional spatial filtering could also be helpful.

2.3. Intracavity Round-Trip Loss and Accumulated Phase Determination

Figure 2 shows the complex electric fields at the input coupler (IC) of the enhancement cavity in the steady state. For each enhanced frequency, the single-round-trip power attenuation

#132118 - $15.00 USD Received 22 Jul 2010; revised 30 Sep 2010; accepted 16 Oct 2010; published 1 Dec 2010

and accumulated phase are denoted by $A(\omega)$ and $\theta(\omega)$, respectively. One cavity round trip of the circulating electric component $\widetilde{E}_c(\omega)$ can be completely described by its multiplication by $\sqrt{A(\omega)}\exp[j\theta(\omega)]$. Thus, the desired quantities, fully describing the single-round-trip propagation, are the frequency-resolved quantities $A(\omega)$ and $\theta(\omega)$.

Let $R(\omega)$ denote the IC power reflectivity, such that a reflection on the cavity side at the IC implies the multiplication of the impinging electric field by $\sqrt{R(\omega)}$. Let $T(\omega)$ denote the IC power transmission. Note that we treat $R(\omega)$ and $T(\omega)$ as real functions by including the spectral phase affects at the IC into $\theta(\omega)$. Resonant enhancement requires the constructive interference of the intracavity field reflected by the IC, i.e., $\sqrt{R(\omega)}\widetilde{E}_c(\omega)\sqrt{A(\omega)}\exp[j\theta(\omega)]$ with the portion of the input field transmitted through the IC, i.e., $\sqrt{T(\omega)}\widetilde{E}_i(\omega)$. In the steady state, the sum of these two interfering fields equals $\widetilde{E}_c(\omega)$:

$$\widetilde{E}_c(\omega) = \sqrt{R(\omega)}\widetilde{E}_c(\omega)\sqrt{A(\omega)}e^{j\theta(\omega)} + \sqrt{T(\omega)}\widetilde{E}_i(\omega) \tag{2}$$

$$\Leftrightarrow \widetilde{H}(\omega) = \frac{\widetilde{E}_c(\omega)}{\widetilde{E}_i(\omega)} = \frac{\sqrt{T(\omega)}}{1-\sqrt{R(\omega)A(\omega)}\exp[j\theta(\omega)]}. \tag{3}$$

Equation (3) can be rewritten as:

$$\sqrt{A(\omega)}e^{j\theta(\omega)} = \frac{1}{\sqrt{R(\omega)}}\left(1-\frac{\sqrt{T(\omega)}}{|\widetilde{H}(\omega)|}e^{-j\phi(\omega)}\right). \tag{4}$$

The right-hand side of Eq. (4) contains quantities, which can be independently measured, while the left-hand side contains the desired quantities. Note that Eqs. (3) and (4), evaluated at the frequencies of the seeding comb, hold for both linear and nonlinear enhancement. However, in the nonlinear case the model given by Eq. (3) only describes the effect of the intracavity nonlinearity on the enhancement of the seeding field and it does not allow any direct conclusion on the nature of the nonlinear effect in question. Moreover, the dependence of $R(\omega)$, $T(\omega)$, $A(\omega)$ and / or $\theta(\omega)$ on the intracavity electric field may turn Eq. (3) into a transcendental equation. However, in the steady state, the frequency-dependent quantity $\widetilde{H}(\omega)$, interpreted as the ratio of the circulating to the incoming fields rather than a linear transfer function, allows for a full description of the intracavity propagation in terms of an amplitude attenuation, i.e. loss, and accumulated phase per round trip.

In order to complete the determination of $A(\omega)$ and $\theta(\omega)$ using Eq. (4), we need to address the measurement of $R(\omega)$ and $T(\omega)$. Here, we assume a lossless IC, i.e. $T(\omega) = 1 - R(\omega)$, as well as the absence of nonlinear processes in the IC. In most practical cases, these assumptions describe the IC behavior very precisely. The IC reflectivity R can be accurately determined with a spectrally resolved ring-down measurement. This technique is well-known and does not require a resonant cavity. Therefore, we assume that the values of $R(\omega)$ and $T(\omega)$ are known.

While the method described here would work with a continuous-spectrum light source as well, only a tiny fraction of its power would be coupled to the resonent cavity. This would result in a low signal-to-noise ratio and, in addition, intracavity strong-field effects could not be studied. Therefore, we illuminate the cavity with a frequency comb, whose modes can be assumed to be equidistant:

$$\omega_N = N\omega_r + \omega_{CE}. \tag{5}$$

Here, N is the comb mode number, ω_r the laser repetition frequency and ω_{CE} is the carrier-envelope offset frequency [34]. In the context of the laser-cavity lock, the following description of $\theta(\omega)$ is convenient:

$$\theta(\omega) = \tau_C\omega + \psi(\omega) = 2\pi\frac{\omega}{\omega_r} + \psi(\omega), \tag{6}$$

#132118 - $15.00 USD Received 22 Jul 2010; revised 30 Sep 2010; accepted 16 Oct 2010; published 1 Dec 2010

where $\tau_C = 2\pi/\omega_r$ is the round trip group delay, measured at the optical frequency used to lock the laser, while $\psi(\omega)$ is a residual term, describing the intracavity dispersion. Note that a simple cavity length change, e.g. by slightly displacing mirror M7, influences only the group-delay term in Eq. (6), while $\psi(\omega)$ remains unaffected. At each frequency of the seeding comb, the cavity round trip phase is:

$$\theta(\omega_N) \quad = \quad 2\pi N + 2\pi\frac{\omega_{CE}}{\omega_r} + \psi(\omega_N). \tag{7}$$

The first term in the above expression is a multiple of 2π for all considered frequencies and, therefore, irrelevant for the analysis that follows. The second term is a constant phase offset, which can be manually tuned by slightly varying the seed oscillator optical pump power (which influences ω_{CE}) and / or the cavity length (which influences ω_r). This degree of freedom allows for the selection of the enhanced spectral range. The cavity group delay dispersion is given by

$$\mathrm{GDD}(\omega) = \frac{\partial^2\theta}{\partial\omega^2} = \frac{\partial^2\psi}{\partial\omega^2} \tag{8}$$

and does not depend on the chosen offset ω_{CE}/ω_r. Therefore, the GDD information can be obtained by differentiating twice the retrieved intracavity phase for arbitrary offsets. In the particular case of large GDD, leading to a truncation of the enhanced spectrum due to the mismatch of the cavity free spectral range and the seeding frequency comb spacing, the dispersion information over the entire seeding spectrum can be obtained by "stitching" together several measurements for different offsets ω_{CE}/ω_r. In doing so, the knowledge of the phase offset is not necessary.

2.4. Sensitivity Enhancement due to the Resonant Cavity

SSI has been successfully employed for sensitive measurements of linear [20, 25, 26] and nonlinear [24, 27–29] phase effects. The main difference between our technique and earlier works is the resonant enhancement cavity implemented in the interferometer sample arm. This significantly increases both the effect on the pulse caused by the investigated light-matter interaction and the peak / average power available for the interaction in the cavity.

Intracavity phase effects are maximally magnified in the spectral range which is also maximally power-enhanced, which we will refer to as the maximally enhanced range. By varying ω_{CE} and / or ω_r, as explained in the previous section, the maximally enhanced range can be selected within the seed pulse spectrum, see Eq. (7). In this spectral region, $|\theta(\omega)|$ and $|\phi(\omega)| \ll 1$ holds, and we can Taylor-expand equation (3) up to the linear terms of θ and ϕ:

$$\left|\widetilde{H}(\omega)\right| \exp[j\phi(\omega)] \quad \approx \quad \frac{\sqrt{T(\omega)}}{1-\sqrt{R(\omega)A(\omega)}[1+j\theta(\omega)]} \tag{9}$$

$$\approx \quad \frac{\sqrt{T(\omega)}}{1-\sqrt{R(\omega)A(\omega)}}\left[1+j\theta(\omega)\frac{\sqrt{R(\omega)A(\omega)}}{1-\sqrt{R(\omega)A(\omega)}}\right] \tag{10}$$

$$\approx \quad \frac{\sqrt{T(\omega)}}{1-\sqrt{R(\omega)A(\omega)}}\exp\left[j\theta(\omega)\frac{\sqrt{R(\omega)A(\omega)}}{1-\sqrt{R(\omega)A(\omega)}}\right] \tag{11}$$

$$\Rightarrow \phi(\omega) \quad \approx \quad \frac{\sqrt{R(\omega)A(\omega)}}{1-\sqrt{R(\omega)A(\omega)}}\theta(\omega). \tag{12}$$

Equation (12) shows that in the maximally enhanced region, the SSI-measured phase of the circulating pulse $\phi(\omega)$ corresponds in good approximation to the the intracavity single-round-trip phase $\theta(\omega)$, magnified by a factor $\sqrt{R(\omega)A(\omega)}/[1-\sqrt{R(\omega)A(\omega)}]$. This phase magnification factor can be several orders of magnitude for high-finesse cavities. In our experimental

#132118 - $15.00 USD Received 22 Jul 2010; revised 30 Sep 2010; accepted 16 Oct 2010; published 1 Dec 2010

setup, it exceeds 1000. The magnification from the intracavity round-trip phase $\theta(\omega)$ to the SSI-measured circulating pulse phase $\phi(\omega)$ leads to a significant sensitivity enhancement of our method compared to the conventional SSI.

2.5. Interferometry Data Processing

One axis of the 2-dimensional spectrometer data array represents the wavelength or, equivalently, ω. The second dimension, which we denote by y, is the spatial axis, along the direction of the spectrometer slit. To determine the magnitude $|\widetilde{H}(\omega)|$, we integrate the individual arm measurements along the y-dimension, and obtain the power spectra of the reference and sample arms. The absolute scale of $|\widetilde{H}(\omega)|$ is determined by normalizing the ratio of the integrated areas under the circulating and input spectra to the ratio P_{circ}/P_{in}, where P_{circ} and P_{in} are the measured intracavity circulating power and the input power to the cavity, respectively.

To determine $\phi(\omega)$, we consider the intensity pattern of the interferogram assuming a separation angle α and a time delay $\Delta\tau$ between the interferometer arms and plane phase fronts [21–23]:

$$I(y,\omega) = I_R(y,\omega) + I_S(y,\omega) + 2\sqrt{I_R(y,\omega)I_S(y,\omega)}\cos\left[\phi(\omega) + \omega\Delta\tau + y\frac{\omega}{c}\sin\alpha\right], \qquad (13)$$

where I_R and I_S, represent the intensity distributions of the reference and the sample arms, respectively. Since $I_R(y,\omega)$ and $I_S(y,\omega)$ can be measured, the cosine term in Eq. (13) can be isolated and calculated from the interferogram $I(y,\omega)$. This term oscillates with the frequency $\frac{\omega}{c}\sin\alpha$ along the y-direction and with the frequency $\Delta\tau + \frac{y}{c}\sin\alpha$ along the ω-direction. Note that for the collinear case ($\alpha = 0$) no oscillation takes place along the y-direction. An advantage of SSI with $\Delta\tau = 0$ and $\alpha \neq 0$ over SI is that the spectral envelope along the y-direction usually displays much less structure and is more stable. Therefore, we set the delay $\Delta\tau$ to zero by calibrating the interferometer arms while the cavity is off-resonance. Thus, the isolated cosine term equals $\cos\left[\phi(\omega) + y\frac{\omega}{c}\sin\alpha\right]$. For each ω, this term represents a cosine oscillation in the y-direction with a phase offset $\phi(\omega)$. The latter is obtained by a cosine fit for each wavelength in the interferogram. Now, $\theta(\omega)$ and $A(\omega)$ are retrieved directly from Eq. (4).

3. Experimental Results and Discussion

3.1. Dispersion Measurement of Air

In a first experiment we measured the dispersion of air inside the cavity for several air pressure values. While the pressure-dependent dispersion of air has been accurately measured with SSI before [25, 26], the aim of this experiment is to validate our enhancement-cavity-based phase measurement method by comparing the retrieved GDD with the Sellmeier model for the dispersion of air [26, 35]. To measure the air pressure we used a Pirani capacitance gauge (Pfeiffer Vacuum, model PCR 260) with a manufacturer specified accuracy between 5% and 15% in the pressure range of our experiment. In order to avoid nonlinear effects in the cavity focus, we seeded the cavity with a low input power of 7 mW and chirped the input pulses to a duration exceeding 2 ps. Since our optical bandwidth is relatively narrow, we restrict the dispersion comparison to the GDD value at 1042 nm. To obtain this value for different air pressure values, we determine $\theta(\omega)$ as described in the previous section and fit a second-order polynomial in ω to a region corresponding to a few nm around 1042 nm, similar to [15].

Figure 3 shows the results. In a), b) and c) interferograms for 200 mbar, 500 mbar and 950 mbar, respectively, are plotted. An increase of the fringe curvature for increasing air pressure can be observed. Part d) shows the intracavity round-trip phase $\theta(\omega)$ including the dispersion from the cavity mirrors and from the intracavity air. To obtain the contribution of air, we

#132118 - $15.00 USD Received 22 Jul 2010; revised 30 Sep 2010; accepted 16 Oct 2010; published 1 Dec 2010

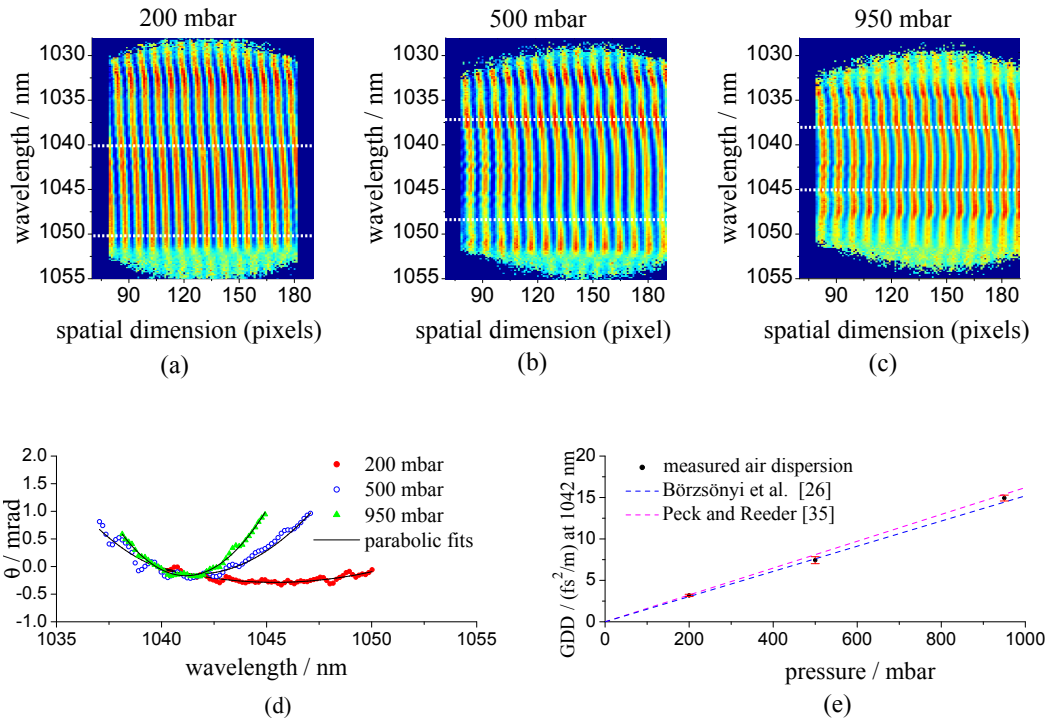

Fig. 3. Dispersion measurement of the air-filled cavity for different air pressure values. a), b) and c) interferograms for 200 mbar, 500 mbar and 950 mbar, respectively. The white lines indicate the fit range for the second-order polynomial. d) retrieved round-trip phases. e) retrieved air GDD in fs^2/m after subtracting the empty cavity round trip GDD and comparison with the Sellmeier models [26, 35]. The error bars show the uncertainty of the quadratic fit, see text for details.

first measure the cavity GDD in vacuum which amounts to -4.5 fs^2. The difference between the measured value and the value calculated by summing up the GDD design values specified by the mirror manufacturer for 7 highly reflecting mirrors and the input coupler is less than 1 fs^2 if we use an optical bandwidth of $\sim$10nm to determine the average GDD. The subtraction of the vacuum cavity GDD from the total GDD yields the values plotted in e). The agreement with the Sellmeier model is excellent. The error bars show the 95% confidence bounds of the quadratic coefficient of the parabolic fit. The calculated relative uncertainties are 4.2%, 5.7% and 2.3% for the 200 mbar, 500 mbar and 950 mbar measurements, respectively. The uncertainty in the fit is mainly given by the oscillating structure on the retrieved phase curves. These oscillations are reproducible for all three measurements, are visible in the interferograms and cause the systematic uncertainty mentioned at the end of Section 2.2.

The parabolic phases in Fig. 3(d) are centered around different wavelength values. This is caused by locking with different constant phase offsets, i.e. different values of the second term in Eq. (7). Nevertheless, the retrieved dispersion values are reproduced, which exemplifies the applicability of our method in the case of relatively large GDD values.

#132118 - $15.00 USD Received 22 Jul 2010; revised 30 Sep 2010; accepted 16 Oct 2010; published 1 Dec 2010

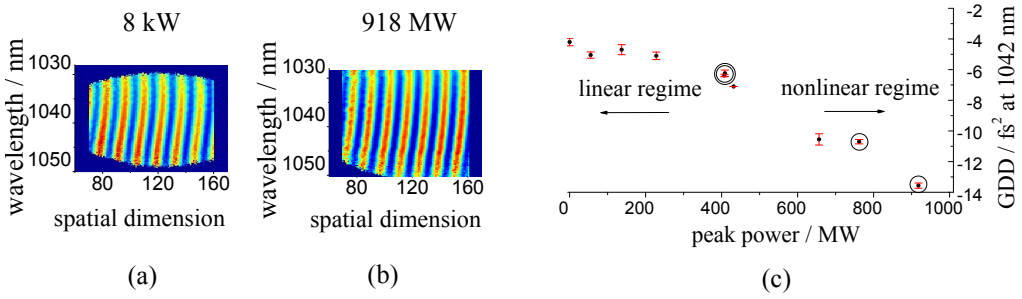

Fig. 4. Peak-power-dependent round trip GDD measurement of the cavity in vacuum. a) and b) interferograms for peak powers $P_{peak} = 8$ kW, and $P_{peak} = 918$ MW, respectively. c) Retrieved GDD values at 1042 nm vs. peak power. The three circled measurements are taken at $P_{circ} = 24$ kW and different pulse durations. The two coinciding double-circled measurements are taken at $P_{circ} = 24$ kW, $\tau_{circ} = 650$ fs and $P_{circ} = 7$ kW, $\tau_{circ} = 200$ fs. The error bars (standard deviation of several measurements) are on the order of 0.2 fs^2.

3.2. Beyond Linear Enhancement: Peak-Power-Dependent Round Trip GDD Measurement

The second experiment demonstrates the applicability of our method beyond the linear enhancement regime. In [19] it was reported that the linear enhancement in our cavity is primarily limited by peak-power-dependent, i.e. nonlinear, effects. In order to activate these effects and to measure the resulting round trip GDD, we performed circulating and peak power scaling experiments of the cavity in vacuum in analogy to [19]. By varying the circulating power in the range 0.9 W $\leq P_{circ} \leq$ 23 kW and the circulating pulse duration in the range 200 fs$\leq \tau_{circ} \leq$ 1.5 ps, we generated intracavity peak powers between 8 kW and almost 1 GW.

The results are plotted in Fig. 4(a) and 4(b) show interferograms for the cases $P_{peak} = 8$ kW, and $P_{peak} = 918$ MW, respectively. The increased curvature of the interference fringes in part (b) can be recognized. The quantitative results of the GDD determination at 1042 nm are shown in pannel (c). Up to approximately 300 MW, we observe a constant GDD value. For the higher peak powers, a deviation from the linear case is evident. The three circled measurements are taken with a constant circulating power of $P_{circ} = 24$ kW and different pulse durations. They constitute a clear indication that the increased absolute GDD is due to an increase of peak power rather than an increase of the time-averaged circulating power. Another evidence for this is given by the two coinciding double-circled measurements which are taken with $P_{circ} = 24$ kW, $\tau_{circ} = 650$ fs and $P_{circ} = 7$ kW, $\tau_{circ} = 200$ fs. The peak power values, at which the determined GDD value starts to deviate from the constant value for the linear regime are in good agreement with the observations in [19]. The exact physical mechanism causing this dispersion requires further study. The error bars indicate a reproducibility of typically 0.2 fs^2.

3.3. Phase Distortions Caused by Air Plasma in the Cavity Focus

Our third experiment addresses qualitatively the highly nonlinear case of a bright air plasma at the intracavity focus. To generate the plasma, we increased the intracavity air pressure up to 8.5 mbar for an input power of 20 W and an intracavity pulse duration of 650 fs. The interferograms for the different pressure values are plotted in Fig. 5. While the autocorrelator measuring the intracavity pulse duration did not indicate any changes over the entire range of pressure values, the interferograms clearly show pressure-dependent phase distortions. A quantitative interpretation of these effects employing an appropriate theoretical model is beyond the scope of this paper. However, this example shows that our method is suited for the sensitive

#132118 - $15.00 USD Received 22 Jul 2010; revised 30 Sep 2010; accepted 16 Oct 2010; published 1 Dec 2010

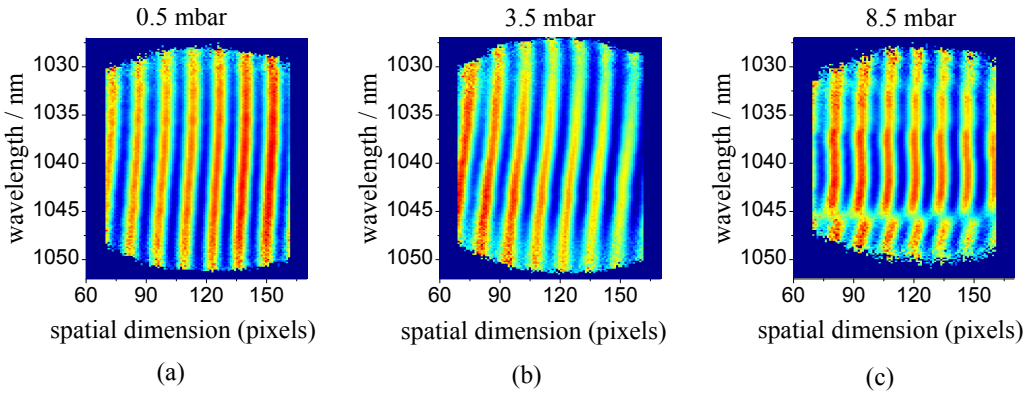

Fig. 5. Interferograms showing phase distortions caused by an air plasma generated in the cavity focus for an input power of 20 W, a pulse duration of 650 fs and air pressure values of a) 0.5 mbar, b) 3.5 mbar and c) 8.5 mbar.

detection and measurement of the influence of highly nonlinear processes on the enhancement behavior of a femtosecond cavity. Conversely, in conjunction with adequate physical models for the nonlinear processes, it offers the prospect of a simple investigation tool with unprecedented precision. With the advent of high-power cavities in the multi-kW regime enhancing sub-picosecond pulses for increasing the net conversion efficiency of nonlinear processes, such as SHG, HHG and THz generation, such studies will become indispensable.

4. Conclusion

We have presented a simple and highly sensitive measurement method for the complex ratio of the field circulating in a fully loaded femtosecond enhancement cavity to the incoming field. This method combines the enhancement of power and phase sensitivity provided by a high-finesse cavity in the resonant state with spatial-spectral interferometry, enabling the highly accurate investigation of both linear enhancement regimes and nonlinear light-matter interaction processes at high intensities and repetition rates. In particular, a round trip GDD determination reproducibility better than 1 fs^2 was demonstrated. The measurement time for the determination of the cavity dispersion over the entire enhanced spectrum amounts to less than 1 second.

The significance of the applicability of this methods beyond the linear enhancement regime is twofold. On the one hand, it allows for the optimization of the cavity for a certain power regime, consisting of e.g. intensity-specific dispersion compensation and / or impedance matching. On the other hand, the measured nonlinear behavior can provide information about the mechanisms causing the nonlinearities, enabling their investigation with a very high accuracy.

Acknowledgements

This work was supported by the Deutsche Forschungsgemeinschaft (DFG) Cluster of Excellence, Munich Centre for Advanced Photonics (MAP) (www.munichphotonics.de) and by the KORONA Max-Planck-Institut fr Quantenoptik (MPQ)/Fraunhofer Institut fr Lasertechnik (ILT) cooperation.

#132118 - $15.00 USD Received 22 Jul 2010; revised 30 Sep 2010; accepted 16 Oct 2010; published 1 Dec 2010